Rakenteiden Mekaniikka (Journal of Structural Mechanics)
Vol. 44, No 3, 2011, pp. 260 – 278

Isogeometric analysis of finite deformation nearly incompressible solids

Kjell Magne Mathisen, Knut Morten Okstad, Trond Kvamsdal and Siv Bente Raknes

Summary. This paper addresses the use of isogeometric analysis to solve finite deformation solid mechanics problems, in which volumetric locking may be encountered. The current work is based on the foundation developed in the project *ICADA* for linear analysis, that herein is augmented with additional capabilities such that nonlinear analysis of finite deformation problems in solid mechanics involving material and geometrical nonlinearities may be performed. In particular, we investigate two mixed forms based on a three-field Hu-Washizu variational formulation, in which displacements, mean stress and volume change are independently approximated. The performance of the mixed forms is assessed by studying two numerical examples involving large-deformation nearly incompressible elasticity and elastoplasticity. The results obtained with NURBS are shown to compare favorable with classical Lagrange finite elements.

Key words: isogeometric analysis, near incompressibility, volumetric locking, mixed formulation, finite deformation, hyperelasticity, plasticity

Introduction

The new paradigm of Isogeometric analysis, introduced by Hughes *et al.* [1, 2], demonstrates that much is to be gained with respect to efficiency, quality and accuracy by replacing traditional finite elements by volumetric NURBS (Non-Uniform Rational B-Splines) elements. By using NURBS—which is standard technology employed in CAD systems—as basis functions in the finite element analysis, one may transfer models from design directly to analysis without any modifications. This reduces the man-hours needed for establishing analysis-suitable finite element meshes, as well as no loss of accuracy in the geometrical description of the object at hand. Thus, using NURBS seems to be a very appealing step forward for finite element analysis. It is therefore natural to investigate the numerical performance of NURBS compared to traditional Lagrange basis functions. We have been doing so for linear elasticity problems and obtained very promising results, and now we start to address this for finite deformation problems.

Two important features with NURBS are its capability to exactly represent conical sections (e.g., circles) and that a regular p-th order NURBS basis is $\mathcal{C}^{p-1}$ continuous. Many industrial solid/structural mechanics problems involve objects where part of the geometry is described by circles or circle segments, and traditionally this has been represented inaccurately by means of low-order Lagrange polynomials, whereas by using NURBS these inaccuracies may be eliminated altogether. Furthermore, in elasticity we have continuous stresses and strains except for at certain singular points, lines or surfaces, i.e. the displacement field is $\mathcal{C}^1$-continuous away from singularities. Classical finite elements based on Lagrange polynomials are only $\mathcal{C}^0$-continuous and this lack of regularity

shows up in discontinuous finite element stress and strain fields across element interfaces, whereas NURBS ($p \geq 2$) may represent this behavior qualitatively correct.

"Locking" is a challenge in linear as well as nonlinear finite element problems: (1) Shear locking in continuum elements, (2) transverse shear locking in Timoschenko beam, and Reissner/Mindlin plate and shell elements, (3) membrane locking in curved shell, membrane or solid elements, and (4) volumetric locking. In the present study we address volumetric locking, often referred to as incompressible locking. This is a challenge when nearly incompressible behavior is prevalent, such as in modeling of dense rubber by hyperelastic materials, as well as in modeling of inelastic problems by large deformation elastic-plastic response of metals or in analysis of undrained soils. Until recently nonlinear finite element structural analysis has been dominated by the use of low-order displacement elements specially designed to avoid volumetric or incompressible locking. Szabó *et al.* [3, 4] claim that the solution is to apply the $p-$method, in which the polynomial order within $\mathcal{C}^0$ elements is increased on a fixed mesh.

More recently the isogeometric approach has formed the basis for overcoming the incompressibility problem. Elguedj *et al.* [5] has addressed this by the $\bar{B}$- and $\bar{F}$-projection methods, for infinitesimal and finite strain problems, respectively. Echter and Bischoff [6] has demonstrated that NURBS in combination with the discrete shear gap method may be used to partly alleviate transverse shear locking and obtain improved accuracy compared to other locking-free elements. For linearized and finite strain elasticity and plasticity, Simo *et al.* [7] showed that $\bar{B}$-projection methods may be derived from a three-field variational formulation. More recently Taylor [8] demonstrated that NURBS may be used to improve the performance of two-dimensional mixed solid elements based on a three-field variational formulation. The latter work forms the basis for the current study, where we adopt two mixed formulations based on a three-field Hu-Washizu variational formulation, originally presented by Simo *et al.* [7], later extended to hyperelastic materials in principal stretches by Simo and Taylor [9], and to general problems by Zienkiewicz and Taylor [10]. These formulations have been implemented into an object-oriented environment for performing isogeometric finite element analysis (*IFEM*), using splines and NURBS as basis functions.

Nonlinear Elasticity

Finite deformation elasticity and elastoplasticity is herein based on a multiplicative split of the deformation gradient into volume-preserving and dilatational parts, which enables exact satisfaction of the constraint condition of isochoric motion. Constitutive models for finite deformation elastoplasticity is formulated in terms of principal stretches [10–12] which have proven to be especially useful in the modeling of elastoplastic materials undergoing large plastic strain.

Compressible neo-Hookean material model

In deriving the constitutive models for finite elasticity, we first assume hyperelastic homogeneous isotropic material behavior for which there exist a free-energy function (stored energy or strain energy function) Ψ that depends on the left Cauchy-Green deformation (*finger*) tensor $\mathbf{b}$

$$\Psi = \Psi(\mathbf{b}) \quad \text{with} \quad \mathbf{b} = \mathbf{F}\mathbf{F}^T \quad \text{and} \quad \mathbf{F} = \mathbf{I} + \frac{\partial \mathbf{u}}{\partial \mathbf{X}}, \tag{1}$$

where $\mathbf{F}$ is the deformation gradient, $\mathbf{u}$ is the displacement and $\mathbf{I}$ is the 2nd order unit tensor. Isotropy implies that Cauchy stresses $\boldsymbol{\sigma}$ may be derived from the three invariants of $\mathbf{b}$

$$\boldsymbol{\sigma} = \frac{2}{J}\frac{\partial \Psi}{\partial \mathbf{b}} = \frac{2}{J}\left(\Psi_I \mathbf{b} + 2\Psi_{II}\mathbf{b}^2 + J^2\Psi_{III}\mathbf{I}\right), \tag{2}$$

where $\Psi_I, \Psi_{II}, \Psi_{III}$ are the derivatives of Ψ with respect to the invariants of $\mathbf{b}$, and $J = \det \mathbf{F}$ the determinant of the deformation gradient. For hyperelastic materials exhibiting a completely different volumetric and isochoric response, the free-energy function may be additively decomposed into a volume-changing (dilatational) part, and a volume-preserving (isochoric) part

$$\Psi(J, \mathbf{b}) = \Psi^{\text{dil}}(J) + \Psi^{\text{iso}}(J, \mathbf{b}). \tag{3}$$

The dilatational part is here expressed in terms of J

$$\Psi^{\text{dil}}(J) = \lambda U(J) = \frac{1}{2}\lambda \left(\ln J\right)^2, \tag{4}$$

and the isochoric part is expressed in terms of J and the finger tensor $\mathbf{b}$

$$\Psi^{\text{iso}}(J, \mathbf{b}) = \frac{1}{2}\mu\left(\text{tr}\mathbf{b} - 3\right) - \mu \ln J, \tag{5}$$

where λ and μ are the Lamé parameters that may be derived from Young's modulus, E, and Poisson's ratio, ν, by

$$\lambda = \frac{\nu E}{(1+\nu)(1-2\nu)} \quad \text{and} \quad \mu = \frac{E}{2(1+\nu)}. \tag{6}$$

Thus, as $\nu \to \frac{1}{2}$, $\lambda \to \infty$. The limit value $\nu = \frac{1}{2}$ thus represents incompressibility.

Cauchy stresses are obtained from the first derivatives of Ψ^{dil} and Ψ^{iso}

$$\sigma_{ij} = \sigma_{ij}^{\text{dil}} + \sigma_{ij}^{\text{iso}} = \left(\lambda\frac{\partial U}{\partial J} + \frac{\partial \Psi^{\text{iso}}}{\partial J}\right)\delta_{ij} + \frac{2}{J}b_{ij}\frac{\partial \Psi^{\text{iso}}}{\partial I} = \frac{1}{J}\left[\mu b_{ij} + \left(\lambda \ln J - \mu\right)\delta_{ij}\right], \tag{7}$$

where $I = \text{tr}\mathbf{b} = b_{kk}$ is the first invariant of $\mathbf{b}$.

Spatial tangent moduli are similarly obtained from the second derivatives

$$c_{ijkl} = c_{ijkl}^{\text{dil}} + c_{ijkl}^{\text{iso}} = \frac{1}{J}\left[\lambda\delta_{ij}\delta_{kl} + 2\left(\mu - \lambda \ln J\right)\mathcal{I}_{ijkl}\right], \tag{8}$$

where $\mathcal{I}_{ijkl} = \frac{1}{2}\left[\delta_{ik}\delta_{jl} + \delta_{il}\delta_{jk}\right]$.

Modified neo-Hookean material model

Materials with rubber-like behavior are characterized by a relatively low shear modulus and high bulk modulus, i.e., they are nearly incompressible while highly deformable when sheared. For such materials it is convenient to make a multiplicative split of the deformation gradient into a dilatational and isochoric part

$$\mathbf{F} = \mathbf{F}^{\text{dil}}\mathbf{F}^{\text{iso}} \quad \begin{cases} \mathbf{F}^{\text{dil}} = J^{1/3}\mathbf{I} & \Rightarrow \quad \det \mathbf{F}^{\text{dil}} = \det \mathbf{F} = J \\ \mathbf{F}^{\text{iso}} = J^{-1/3}\mathbf{F} & \Rightarrow \quad \det \mathbf{F}^{\text{iso}} = 1 \end{cases}, \tag{9}$$

where the latter defines an isochoric motion. A modified deformation gradient $\bar{\mathbf{F}}$ is obtained by replacing J with the scalar parameter $\bar{J}$ in the dilatational part, resulting in

$$\bar{\mathbf{F}} = \bar{\mathbf{F}}^{\mathrm{dil}}\mathbf{F}^{\mathrm{iso}} = \left(\frac{\bar{J}}{J}\right)^{1/3}\mathbf{F} \quad \text{where} \quad \bar{\mathbf{F}}^{\mathrm{dil}} = \bar{J}^{1/3}\mathbf{I} \Rightarrow \det\bar{\mathbf{F}} = \bar{J}. \tag{10}$$

Using the multiplicative split the isochoric part of the finger tensor becomes

$$\bar{\mathbf{b}} = \mathbf{b}^{\mathrm{iso}} = \mathbf{F}^{\mathrm{iso}}(\mathbf{F}^{\mathrm{iso}})^T = J^{-2/3}\mathbf{b}, \tag{11}$$

and again has unit volume change. The isochoric part of the free-energy function may now be written in terms of the modified invariant $\bar{I} = \mathrm{tr}\bar{\mathbf{b}} = J^{-2/3}\mathrm{tr}\mathbf{b}$

$$\Psi(J, \bar{I}) = \Psi^{\mathrm{dil}}(J) + \Psi^{\mathrm{iso}}(\bar{I}), \tag{12}$$

where

$$\begin{aligned} \Psi^{\mathrm{dil}}(J) &= \kappa U(J) = \tfrac{1}{4}\kappa\left(J^2 - 1 - 2\ln J\right), \\ \Psi^{\mathrm{iso}}(\bar{I}) &= \tfrac{1}{2}\mu\left(\bar{I} - 3\right), \end{aligned} \tag{13}$$

and where κ and μ are equivalent to the small strain bulk and shear moduli, respectively. The volumetric part of the Cauchy stresses is proportional to $U(J)$ which for the above volumetric behavior gives rise to the hydrostatic pressure

$$\sigma_{ij}^{\mathrm{dil}} = \kappa\frac{\partial U}{\partial J}\delta_{ij} = \frac{\kappa}{2J}(J^2 - 1)\delta_{ij}, \tag{14}$$

while the deviatoric part now may be expressed in terms of the modified deformation tensor $\bar{b}_{ij}$

$$\sigma_{ij}^{\mathrm{iso}} = \frac{\mu}{J}\bar{b}_{ij}^{\mathrm{d}} \quad \text{where} \quad \bar{b}_{ij}^{\mathrm{d}} = \bar{b}_{ij} - \frac{1}{3}\delta_{ij}\bar{b}_{kk}. \tag{15}$$

Current spatial tangent moduli for the modified neo-Hookean material model are again obtained from the second derivatives of the free-energy function w.r.t. J and $\bar{I}$

$$c_{ijkl} = c_{ijkl}^{\mathrm{dil}} + c_{ijkl}^{\mathrm{iso}}, \tag{16}$$

where

$$\begin{aligned} c_{ijkl}^{\mathrm{dil}} &= \tfrac{\kappa}{J}\left[J^2\delta_{ij}\delta_{kl} + (1 - J^2)\mathcal{I}_{ijkl}\right], \\ c_{ijkl}^{\mathrm{iso}} &= \tfrac{2\mu}{3J}\left[\bar{b}_{mm}(\mathcal{I}_{ijkl} - \tfrac{1}{3}\delta_{ij}\delta_{kl}) - \delta_{ij}\bar{b}_{kl}^{\mathrm{d}} - \bar{b}_{ij}^{\mathrm{d}}\delta_{kl}\right]. \end{aligned} \tag{17}$$

Mixed Formulation

Mixed elements are often used to accommodate the volume constraint in incompressible material problems. They are designed to model material behavior with high incompressibility, such as fully or nearly incompressible hyperelastic materials and nearly incompressible elastoplastic materials undergoing large plastic strain. In order to satisfy the extra constraints exactly, the displacements have to be augmented by two additional unknowns, the pressure and the volume change parameters, respectively.

A three-field mixed variational form

For many constitutive models, such as hyperelasticity that can have multiple deformation states for the same stress level, it is convenient to use a three-field mixed Hu-Washizu variational form to overcome volumetric locking. A three-field mixed approximation has led to successful lower-order solid elements that can be used in finite deformation elasticity problems exhibiting compressible and/or nearly incompressible behavior for a large class of materials. Assuming an independent approximation of the displacement $\mathbf{u}$, the hydrostatic pressure p and the volume change parameter θ, the standard displacement form of the variational problem may be augmented to the following form [7, 8, 10]

$$\Pi(\mathbf{u}, p, \theta) = \int_{\Omega} \Psi(J, \bar{\mathbf{b}}) \mathrm{d}\Omega + \int_{\Omega} p(J - \bar{J}) \mathrm{d}\Omega - \Pi_{\text{ext}}, \tag{18}$$

where Π_{ext} includes effects of body forces and surface tractions. The parameter p is here a Lagrange multiplier that constrains the determinant of the deformation gradient, J, to its independent representation, $\bar{J}$. It may be identified as the Cauchy mean or hydrostatic stress

$$\sigma_{ij}^{\text{dil}} = p\delta_{ij}. \tag{19}$$

For computations, we let $\bar{J}$ be related to the volume change parameter θ through

$$\bar{J} = 1 + \theta \Rightarrow \theta = 0 \quad \text{in} \quad \mathcal{C}_0, \tag{20}$$

such that no initial values need to be assigned to θ in the initial configuration. Note that the deformation gradient $\mathbf{F}$ is replaced by $\bar{\mathbf{F}} = \left(\bar{J}/J\right)^{1/3} \mathbf{F}$, and $J = \det \mathbf{F}$ is replaced by $\bar{J}$, in the expression for $\bar{\mathbf{b}}$ in equation (11), that defines the strain energy function $\Psi(J, \bar{\mathbf{b}})$ in equation (18)

$$\bar{\mathbf{b}} = \bar{J}^{-2/3} \bar{\mathbf{F}} \bar{\mathbf{F}}^T = J^{-2/3} \mathbf{b}. \tag{21}$$

Discrete form

In a standard isoparametric finite element solution, classical Lagrange polynomials define the basis functions, N_a, used to parameterize reference coordinates, $\mathbf{X}$, and displacements, $\mathbf{u}$

$$\mathbf{X} = \sum_{a=1}^{n_u} N_a(\boldsymbol{\xi}) \tilde{\mathbf{X}}_a \quad \text{and} \quad \mathbf{u} = \sum_{a=1}^{n_u} N_a(\boldsymbol{\xi}) \tilde{\mathbf{u}}_a, \tag{22}$$

where $\tilde{\mathbf{X}}_a$ and $\tilde{\mathbf{u}}_a$ denote nodal reference coordinates and displacements, respectively, and $\boldsymbol{\xi}$ are the parametric coordinates. For isogeometric elements, geometry and displacements are parameterized by tensor product NURBS basis functions

$$\begin{aligned} \mathbf{X} &= \sum_{i=1}^{n_1} \sum_{j=1}^{n_2} \sum_{k=1}^{n_3} N_i^p(\xi) N_j^q(\eta) N_k^r(\zeta) \tilde{\mathbf{X}}_{ijk}, \\ \mathbf{u} &= \sum_{i=1}^{n_1} \sum_{j=1}^{n_2} \sum_{k=1}^{n_3} N_i^p(\xi) N_j^q(\eta) N_k^r(\zeta) \tilde{\mathbf{u}}_{ijk}, \end{aligned} \tag{23}$$

where $\tilde{\mathbf{X}}_{ijk}$ and $\tilde{\mathbf{u}}_{ijk}$ are the reference coordinates and the displacements of control points, p, q and r are the order of, and n_1, n_2 and n_3 denote the number of basis functions N_i^p, N_j^q and N_k^r, in the ξ, η and ζ-directions, respectively.

If we approximate the volume change θ and the pressure p by interpolation functions $\mathbf{L}$ and $\mathbf{M}$ in reference coordinates $\mathbf{X}$, respectively

$$\theta = \sum_{b=1}^{n_\theta} L_b(\mathbf{X})\tilde{\theta}_b = \mathbf{L}\tilde{\boldsymbol{\theta}} \quad \text{and} \quad p = \sum_{b=1}^{n_p} M_b(\mathbf{X})\tilde{p}_b = \mathbf{M}\tilde{\mathbf{p}}, \tag{24}$$

the linearized discrete form of the variational equation takes the form

$$\begin{bmatrix} \mathbf{K}_{uu} & \mathbf{K}_{u\theta} & \mathbf{K}_{up} \\ \mathbf{K}_{\theta u} & \mathbf{K}_{\theta\theta} & \mathbf{K}_{\theta p} \\ \mathbf{K}_{pu} & \mathbf{K}_{p\theta} & \mathbf{0} \end{bmatrix} \begin{Bmatrix} d\tilde{\mathbf{u}} \\ d\tilde{\boldsymbol{\theta}} \\ d\tilde{\mathbf{p}} \end{Bmatrix} = \begin{Bmatrix} \mathbf{R}_u \\ \mathbf{R}_\theta \\ \mathbf{R}_p \end{Bmatrix}. \tag{25}$$

Residuals are expressed as sums over elements as

$$\begin{aligned} \mathbf{R}_u &= \mathbf{f} - \sum_e \int_{\Omega_e} \mathbf{B}^T \widehat{\boldsymbol{\sigma}} \bar{J} \mathrm{d}\Omega, \\ \mathbf{R}_\theta &= \sum_e \int_{\Omega_e} \mathbf{L}^T (\bar{p} - p) \mathrm{d}\Omega, \\ \mathbf{R}_p &= \sum_e \int_{\Omega_e} \mathbf{M}^T (J - \bar{J}) \mathrm{d}\Omega, \end{aligned} \qquad \text{where} \quad \begin{aligned} &\widehat{\boldsymbol{\sigma}} = \bar{\boldsymbol{\sigma}} + \mathbf{m}(\hat{p} - \bar{p}), \\ &\bar{p} = \tfrac{1}{3}\mathbf{m}^T \bar{\boldsymbol{\sigma}}, \\ &\hat{p} = (J/\bar{J})p, \\ &\mathbf{m}^T = [1,1,1,0,0,0]\,, \end{aligned} \tag{26}$$

in which $\mathbf{f}$ is the external force, and adopting the spatial formulation $\mathbf{B}$ is identical to the form of the small deformation strain-displacement matrix [10]. In three dimensions the portion of this matrix associated with a node a is defined by

$$\mathbf{B}_a^T = \begin{bmatrix} N_{a,1} & 0 & 0 & N_{a,2} & 0 & N_{a,3} \\ 0 & N_{a,2} & 0 & N_{a,1} & N_{a,3} & 0 \\ 0 & 0 & N_{a,3} & 0 & N_{a,2} & N_{a,1} \end{bmatrix}. \tag{27}$$

Contrary to the material description where reference coordinates $\mathbf{X}$ are used to compute shape functions and their derivatives, in the spatial description the current configuration coordinates $\mathbf{x}$ are used to compute the derivatives $N_{a,i} = \partial N_a / \partial x_i$. The tangent matrix terms needed to determine $d\tilde{\mathbf{u}}$, $d\tilde{\boldsymbol{\theta}}$ and $d\tilde{\mathbf{p}}$ are given by

$$\begin{aligned} \mathbf{K}_{uu} &= \sum_e \int_{\Omega_e} \mathbf{B}^T \bar{\mathbf{D}}_{\mathrm{d}} \mathbf{B} \bar{J} \mathrm{d}\Omega + \mathbf{K}^G, \\ \mathbf{K}_{u\theta} &= \sum_e \int_{\Omega_e} \mathbf{B}^T \bar{\mathbf{d}} \bar{\mathbf{L}} \bar{J} \mathrm{d}\Omega = \mathbf{K}_{\theta u}^T, \\ \mathbf{K}_{up} &= \sum_e \int_{\Omega_e} \mathbf{B}^T \mathbf{m} \mathbf{M} J \mathrm{d}\Omega = \mathbf{K}_{pu}^T, \\ \mathbf{K}_{\theta\theta} &= \sum_e \int_{\Omega_e} \bar{\mathbf{L}}^T \bar{\mathbf{L}} \bar{J} \mathrm{d}\Omega, \\ \mathbf{K}_{\theta p} &= \sum_e \int_{\Omega_e} \mathbf{L}^T \mathbf{M} \mathrm{d}\Omega = \mathbf{K}_{p\theta}^T. \end{aligned} \tag{28}$$

$\bar{\mathbf{D}}_{\mathrm{d}}$ is the deviatoric part of the expanded material moduli $\bar{\mathbf{D}}$ on matrix form

$$\begin{aligned} &\bar{\mathbf{D}}_{\mathrm{d}} = \mathbf{I}_{\mathrm{d}} \bar{\mathbf{D}} \mathbf{I}_{\mathrm{d}} - \tfrac{2}{3}\left(\mathbf{m}\bar{\boldsymbol{\sigma}}_{\mathrm{d}}^T + \bar{\boldsymbol{\sigma}}_{\mathrm{d}} \mathbf{m}^T\right) + 2\left(\bar{p} - \hat{p}\right)\mathbf{I}_0 - \left(\tfrac{2}{3}\bar{p} - \hat{p}\right)\mathbf{m}\mathbf{m}^T, \\ &\bar{\mathbf{d}} = \tfrac{1}{3}\mathbf{I}_{\mathrm{d}} \bar{\mathbf{D}} \mathbf{m} + \tfrac{2}{3}\bar{\boldsymbol{\sigma}}_{\mathrm{d}}, \qquad \bar{d} = \tfrac{1}{9}(\mathbf{m}^T \bar{\mathbf{D}} \mathbf{m} - 3\bar{p}), \qquad \mathbf{I}_{\mathrm{d}} = \mathbf{I} - \tfrac{1}{3}\mathbf{m}\mathbf{m}^T, \\ &\mathbf{K}_{ab}^G = \int_{\Omega_e} N_{a,i} \bar{\sigma}_{ij} N_{b,j} \mathrm{d}\Omega \mathbf{I}, \qquad \bar{\mathbf{L}} = \mathbf{L}/\bar{J}, \qquad \mathbf{I}_0 = \tfrac{1}{2}\lceil 2,2,2,1,1,1 \rfloor. \end{aligned} \tag{29}$$

To avoid numerical locking the approximations for the primary unknown $\mathbf{u}$, and the constraint variables θ and p, must be selected to satisfy the Babuška–Brezzi condition [13, 14]. For the three-field forms applied in the present study the Babuška–Brezzi condition implies that the displacement space has to be larger than the corresponding spaces for the volumetric change and the pressure fields that may be of equal size. In order to predict the propensity of volumetric locking we define the constraint ratio [15]

$$r_c = \frac{n_u}{n_p} = \frac{n_u}{n_\theta}, \tag{30}$$

where n_u, n_θ and n_p are the number of unknown displacement $\tilde{\mathbf{u}}$, volume $\tilde{\boldsymbol{\theta}}$, and pressure parameters $\tilde{\mathbf{p}}$, respectively. The ideal value of the ratio r_c would then be the ratio between the number of equilibrium equations divided by the number of incompressibility conditions for the governing system of partial differential equations, i.e. the ratio between the number of space dimensions, n_{sd}, and 1, respectively. Thus, in two dimensions, the ideal ratio would be $r_c = 2$. If $r_c < 2$ volumetric locking may be anticipated, and if $r_c \leq 1$ severe locking may be encountered.

The above count condition is a necessary condition to avoid singularity, but not sufficient to avoid incompressibility locking. However, it provides a guideline to construct possible approximations that are not over-constrained.

In the current study we have implemented and studied two different constraint approximations based on the three-field mixed variational form:

Q_p/P_{p-1} : The discretization of $\mathbf{u}$ is of degree p with $\mathcal{C}^{p-1}$ continuity within each "patch", while the discretization of θ and p is discontinuous between each knot-span and of degree $p-1$.

Q_p/Q_{p-1} : The discretization of $\mathbf{u}$ is of degree p with $\mathcal{C}^{p-1}$ continuity, whereas the discretization of θ and p is of degree $p-1$ with $\mathcal{C}^{p-2}$ continuity within each "patch", respectively.

Discontinuous $\theta - p$ approximations

For the Q_p/P_{p-1} approximation the discretizations for θ and p are identical ($\mathbf{L} = \mathbf{M}$) and assumed to be discontinuous between contiguous elements. Hence, the residuals $\mathbf{R}^e_\theta$ and $\mathbf{R}^e_p$ may be expanded in individual elements, which imply that $\tilde{\boldsymbol{\theta}}$ and $\tilde{\mathbf{p}}$ may be condensed out on the element level. For NURBS approximations, however, θ and p are assumed to be discontinuous between contiguous knot-spans. Hence, for NURBS approximations the residuals $\mathbf{R}^e_\theta$ and $\mathbf{R}^e_p$ are expanded in individual knot-spans. The linearized form may then be reduced to

$$\bar{\mathbf{K}}_{uu}\tilde{\mathbf{u}} = \mathbf{R}_u, \tag{31}$$

where

$$\bar{\mathbf{K}}_{uu} = \mathbf{K}_{uu} + \mathbf{K}_{up}\mathbf{K}^{-1}_{\theta p}\mathbf{K}_{\theta\theta}\mathbf{K}^{-1}_{p\theta}\mathbf{K}_{pu} - \mathbf{K}_{u\theta}\mathbf{K}^{-1}_{\theta p}\mathbf{K}_{pu} - \mathbf{K}_{up}\mathbf{K}^{-1}_{\theta p}\mathbf{K}_{\theta u}. \tag{32}$$

An efficient procedure to compute the reduced tangent, that requires the determination of the inverse of $\mathbf{K}^e_{\theta p}$, may be found in [10].

The lowest order Q_p/P_{p-1} approximation is with $p = 1$, for which NURBS and Lagrange approximation results in the same Q_1/P_0 element. In two and three dimensions, displacements $\mathbf{u}$ are represented by the bilinear and the trilinear Lagrange interpolation polynomials (that are identical to NURBS of order $p = 1$), respectively, while θ and p are

approximated by functions that are constant. Although the Q_1/P_0 element fails to satisfy the Babuška–Brezzi condition condition for some mesh configurations (checkerboard mode), it is the most widely used element for large deformation analysis of industrial problems for nearly incompressible and incompressible materials.

We also note that the constraint ratio, r_c, indicate that the discontinuous $\theta - p$ NURBS approximations will experience severe volume locking as the polynomial order of the approximation functions is increased. Numerical results, however, justify that as the ratio λ/μ is large but not infinite, the Q_p/P_{p-1} approximations will not experience severe volumetric locking, even for values up to polynomial order $p = 4$.

Continuous $\theta - p$ approximations

In contrast to the Q_p/P_{p-1} approximation where θ and p are approximated locally, the θ and p approximations are continuous between contiguous elements for Q_p/Q_{p-1}. With NURBS approximations this implies that θ and p have one control point less in each knot direction compared to the displacement

$$\begin{aligned} \theta &= \sum_{i=1}^{\bar{n}_1} \sum_{j=1}^{\bar{n}_2} \sum_{k=1}^{\bar{n}_3} N_i^p(\xi) N_j^q(\eta) N_k^r(\zeta) \tilde{\theta}_{ijk}, \\ p &= \sum_{i=1}^{\bar{n}_1} \sum_{j=1}^{\bar{n}_2} \sum_{k=1}^{\bar{n}_3} N_i^p(\xi) N_j^q(\eta) N_k^r(\zeta) \tilde{p}_{ijk}, \end{aligned} \tag{33}$$

where $\bar{n}_1$, $\bar{n}_2$ and $\bar{n}_3$ are the number of control points defining $\tilde{\theta}_{ijk}$ and $\tilde{p}_{ijk}$, respectively.

The NURBS approximation spaces for a one-dimensional patch of four elements is given in Figure 1 for $p = 1, 2$ and 3. In general the Q_p/Q_{p-1} approximation may attain $\mathcal{C}^{p-1}/\mathcal{C}^{p-2}$ continuity for displacements/constraint variables, respectively, for all values of $p > 1$.

It is also noted that elimination of the volume change parameters $\tilde{\boldsymbol{\theta}}$ locally would lead to a form with displacements and hydrostatic pressure continuous, while the volume change remains discontinuous. This would have resulted in a more efficient formulation in terms of computational effort keeping the accuracy at almost the same level [8].

Numerical Studies

The performance of the three different forms; (1) One-field standard displacement Q_p formulation, (2) three-field mixed Q_p/P_{p-1} formulation with discontinuous p and θ, and (3) three-field mixed Q_p/Q_{p-1} formulation with continuous p and θ, is numerically assessed on two benchmark test problems. For both problems the above three forms with NURBS are compared to results obtained with classical Lagrange Q_p approximation. The accuracy and the convergence characteristics of the formulations are assessed in the finite deformation regime. The numerical simulations involve finite deformation nearly incompressible elastic and elastoplastic problems in plane strain conditions. For the elastic problem the response is governed by a modified neo-Hookean material model, while the elastoplastic response is governed by a finite deformation elastoplastic model with a J_2 yield surface.

Cook's membrane problem in the nonlinear regime

In the first example, a nonlinear extension of the well-known Cook's membrane problem is considered. This problem has frequently been used to assess finite elements under

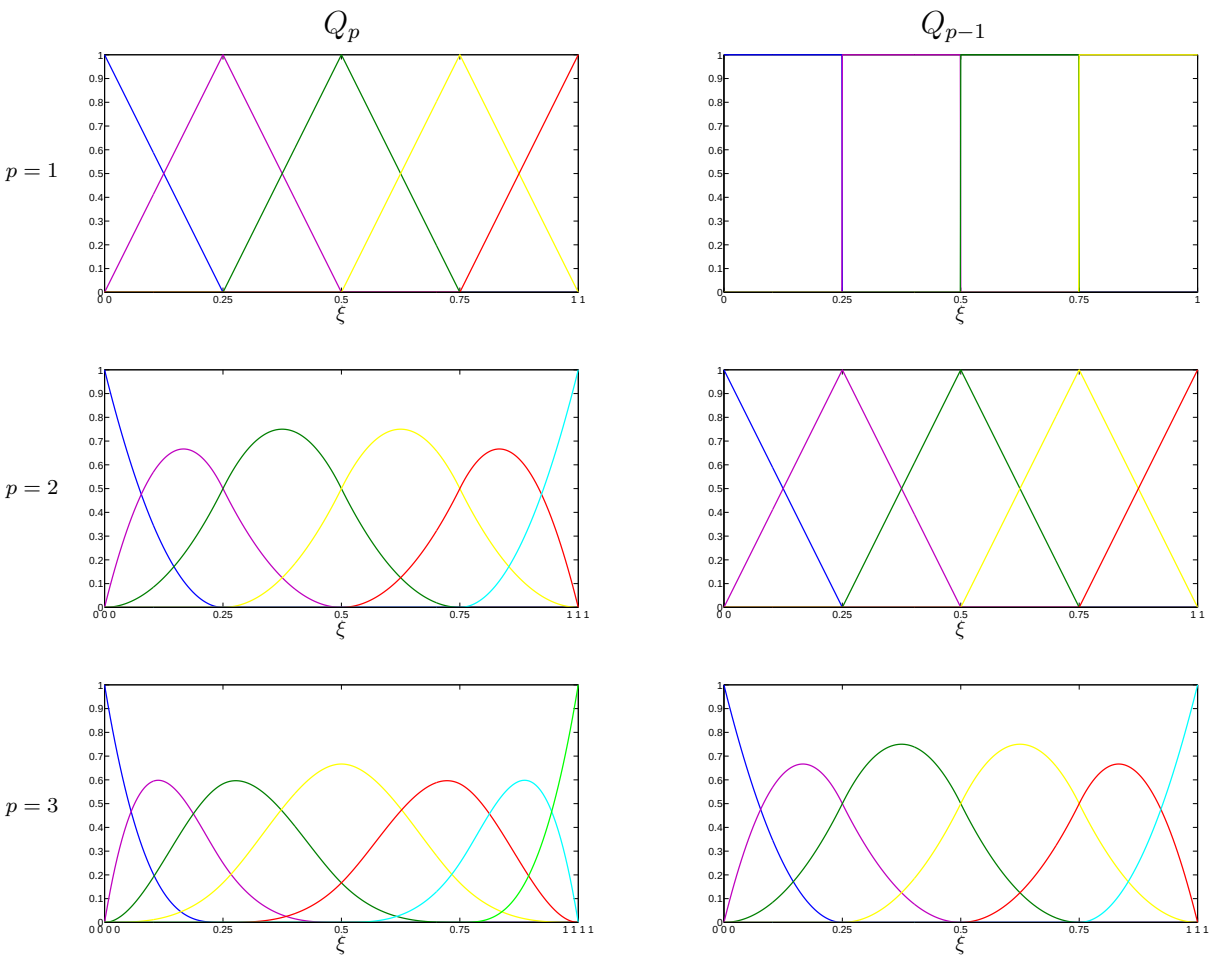

Figure 1. Basis functions Q_p/Q_{p-1}; $p = 1, 2$ and 3, for a one-dimensional patch of four elements.

combined bending and shear for linear elastic materials. More recently this example has been used to validate and test the performance of formulations for incompressible or nearly incompressible materials in both small and large deformation [16–26]. Its extension to finite strain plasticity was proposed by Simo and Armero [27], and has later also been studied by others [5, 28, 29].

The problem consists of a tapered panel clamped on one end and subjected to a uniform shearing load on the opposite end. Figure 2 depicts the initial geometry, loading and boundary conditions of this problem. The problem has been assessed in the finite deformation regime with two different material models. First, we consider the modified neo-Hookean material model with strain energy function defined by equations (12) and (13). Second, we consider a J_2-finite strain model expressed in principal stretch form [10–12], which represent an hyperelastic extension of J_2-flow theory with a modified neo-Hookean model for the elastic part, and nonlinear isotropic hardening with an associative flow rule based on von Mises yield criterion with isotropic hardening following a saturation law for the plastic part [12, 30, 31]. The nonlinear isotropic hardening rule is defined in terms of the yield stress in uniaxial tension

$$\sigma_y = \sigma_\infty + (\sigma_0 - \sigma_\infty)\exp(-\beta e_p) + \sqrt{\frac{2}{3}} h e_p, \tag{34}$$

where σ_0 is the initial yield stress, σ_∞ is the residual yield stress, β is the saturation exponent, h is the isotropic hardening coefficient, and e_p is the equivalent plastic strain.

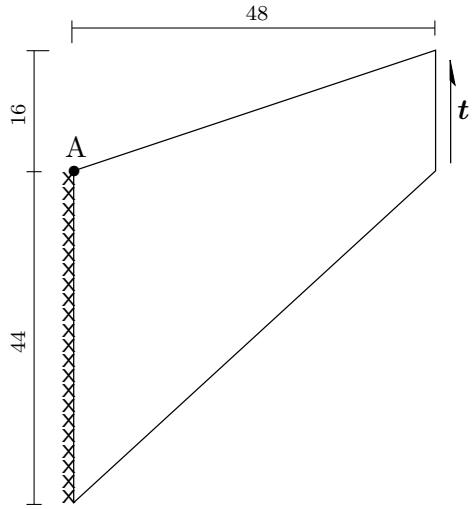

Figure 2. Cook's membrane problem: Geometry, loading and boundary conditions.

The material parameters are those used in the study by Simo and Armero [27], and are presented in Table 1.

The panel is parameterized by a single NURBS patch and analyzed using quadratic, cubic, and quartic NURBS as basis functions only, since for $p = 1$ NURBS and Lagrange approximations coincide. We then compare with standard Lagrange Q_p finite elements of corresponding degree. The load is applied over 5 and 20 equally sized load increments for the elastic and elastoplastic material models, respectively. As the analytical solution is not available for either cases, we consider as reference solution the values obtained with a quartic Q_p/Q_{p-1} formulation for the nearly incompressible finite elastic case and a quartic Q_p/P_{p-1} formulation for the case with finite deformation plasticity. Both reference solutions were obtained with a very fine mesh with 5.01×10^5 degrees of freedom (dofs).

In previous studies the vertical displacement of the top right corner of the panel has been considered as the quantity of interest. However, in this study we present the results in terms of the error in energy versus number of dofs, which accounts for the accuracy of the overall solution.

The results for nearly incompressible finite elasticity are presented in Figure 3. From Figure 3a) we observe that except for quadratic NURBS, the NURBS solution is better

Table 1. Cook's membrane problem: Loading and material parameters.

		Nearly incompressible finite elasticity	Finite deformation plasticity
Constant traction	$\boldsymbol{t}$	$100/16 = 6.25$	$5/16 = 0.3125$
Bulk modulus	κ	40.0942×10^4	164.21
Shear modulus	μ	80.1938	80.1938
Initial yield stress	σ_0		0.45
Residual yield stress	σ_∞		0.715
Isotropic hardening	h		0.12924
Saturation exponent	β		16.93

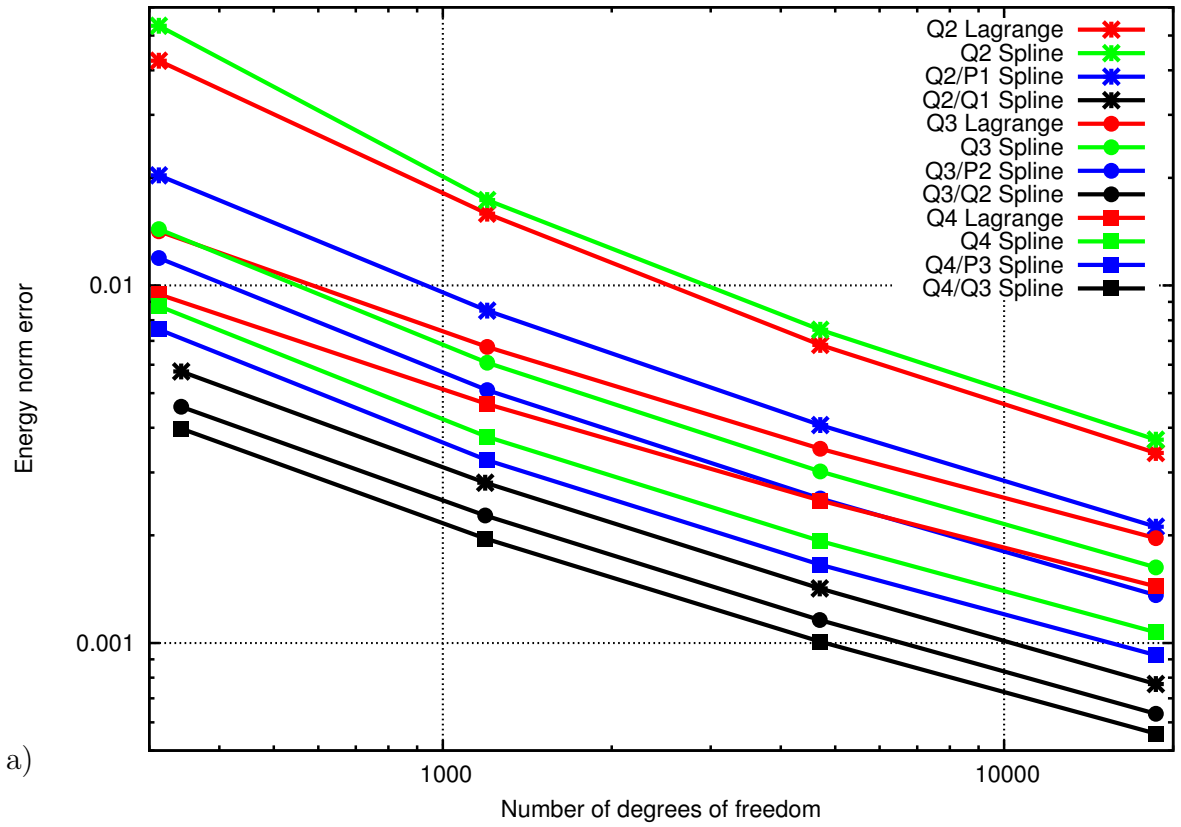

a)

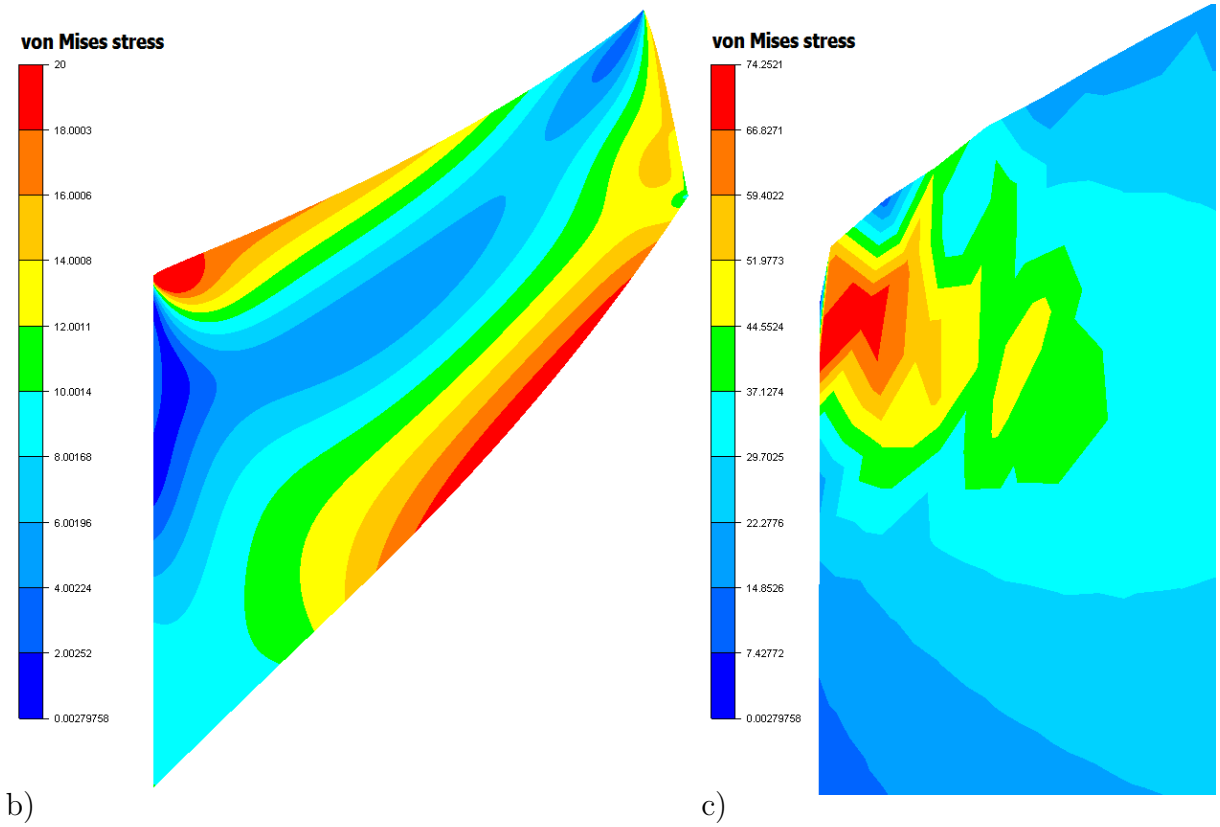

b)

c)

Figure 3. Cook's membrane problem – nearly incompressible finite elasticity: a) Energy norm errors. b) von Mises stress distribution on deformed configuration for the finest mesh with quartic Q_p/P_{p-1} NURBS at the final configuration. b) Close-up view of the von Mises stress distribution around point A.

than the corresponding Lagrange solution with the same polynomial order, and that the difference increases as the polynomial order p of the basis functions is increased. We also notice that for all formulations the solution is improved as p increases. From Table 1 we notice that near incompressibility is achieved with the high ratio between the bulk and shear modulus which is of the order 10^4 for the finite elasticity case, and corresponds to a Poisson's ratio of $\nu = 0.4999$, hence volumetric locking is evident. This explains why the two mixed formulations Q_p/P_{p-1} and Q_p/Q_{p-1} lead to a better approximation compared to the standard displacement Q_p formulation. Figure 3a) also documents that the continuous Q_p/Q_{p-1} mixed formulation outperform the discontinuous Q_p/P_{p-1} mixed formulation in terms of accuracy for all values of p, even though the difference is reduced as p is increased. As the polynomial degree p increases the constraint ratio, r_c, indicate that the Q_p/P_{p-1} formulation will anticipate volumetric locking. This explains the rather poor performance of the discontinuous Q_p/P_{p-1} formulation compared to the continuous Q_p/Q_{p-1} formulation, for which the constraint ratio equals the optimal value, $r_c = 2$, for all values of p.

Figure 3b) shows the von Mises stress distribution obtained with the reference solution at the final configuration. From Figure 3c) we observe that we have a singularity at point A that we do not catch with the coarser meshes. If the convergence study has been extended with even finer meshes it is assumed that the singularity would have caused the curves in Figure 3a) to flatten out when number of dofs is increased.

Figure 4 presents the results for finite deformation plasticity. From Figure 4a) we observe that the NURBS solution is better than the corresponding Lagrange solution with the same polynomial order, for all values of p. As observed for finite elasticity, we notice that the two mixed formulations lead to a better approximation compared to the standard displacement formulation also for finite deformation plasticity. Comparing the two mixed formulations, we observe that the continuous Q_p/Q_{p-1} formulation is more accurate compared to the discontinuous Q_p/P_{p-1} formulation for $p = 2$, nearly coincide for $p = 3$, and less accurate for $p = 4$. Hence, increasing the polynomial order p, the Q_p/P_{p-1} becomes more accurate compared to Q_p/Q_{p-1} for finite deformation plasticity.

Figure 4b) shows the distribution of the equivalent plastic strain obtained with the reference solution at the final configuration. Again as observed for finite elasticity, we observe that we have a singularity at point A, where the equivalent plastic strain $e_p = 8.758$, which is much higher than elsewhere in the domain.

Plain strain localization problem

In the second example, we consider a plane strip subjected to uniform extension and plain strain loading conditions. This is a standard test problem for finite deformation plasticity, and has been studied by a number of authors [8, 25–28, 32, 33]. The same material model is considered as for the Cook's membrane problem − finite deformation plasticity. The geometry and material properties are presented in Figure 5.

In order to trigger necking, an initial geometric imperfection in the form of a linear reduction of the width from its initial value, w, at the top to center width, $w_c = 0.982w$, is prescribed. Only one quarter of the strip is discretized imposing symmetry boundary conditions. The analyses are performed with prescribing a total displacement, $u = 5$, of the top edge in 500 equally sized increments. The analyses are carried out on a discretization consisting of 7×13 grid points with a more refined mesh in the necking area, as shown in Figure 5. In case of Lagrange elements, the number of grid points corresponds

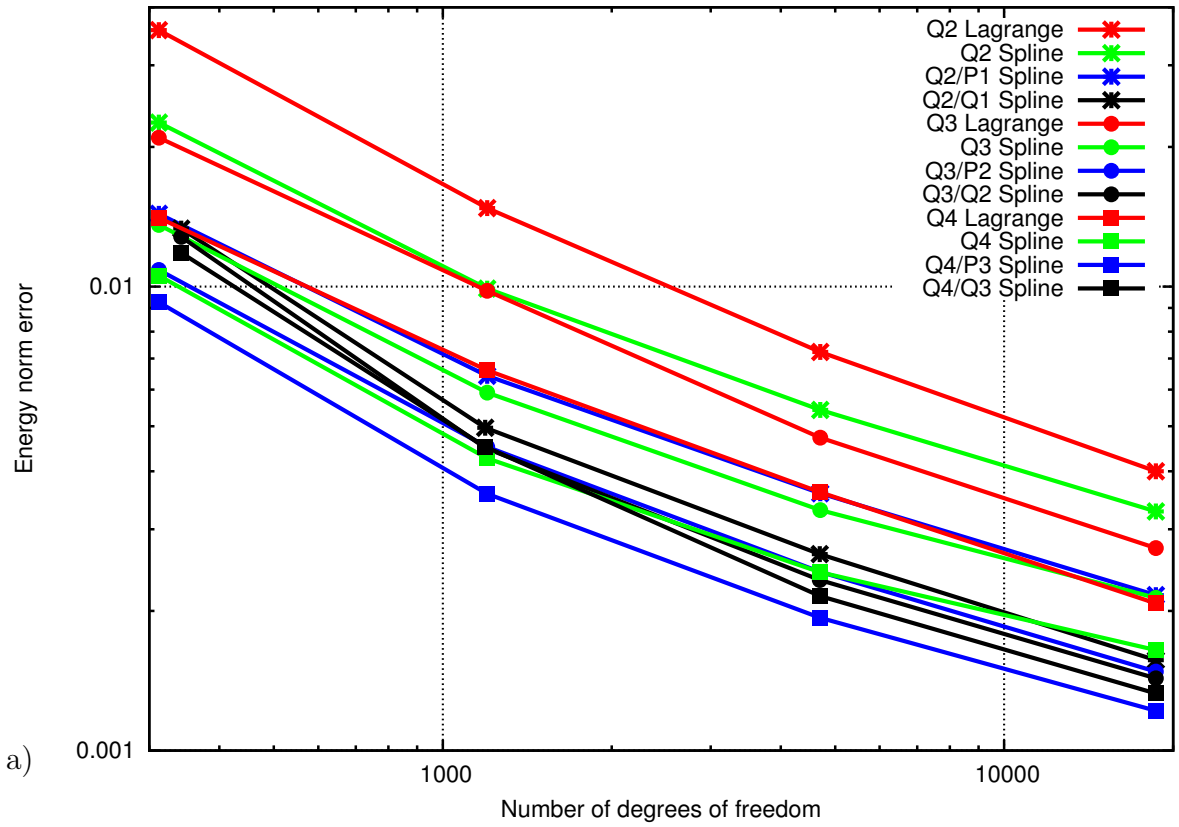

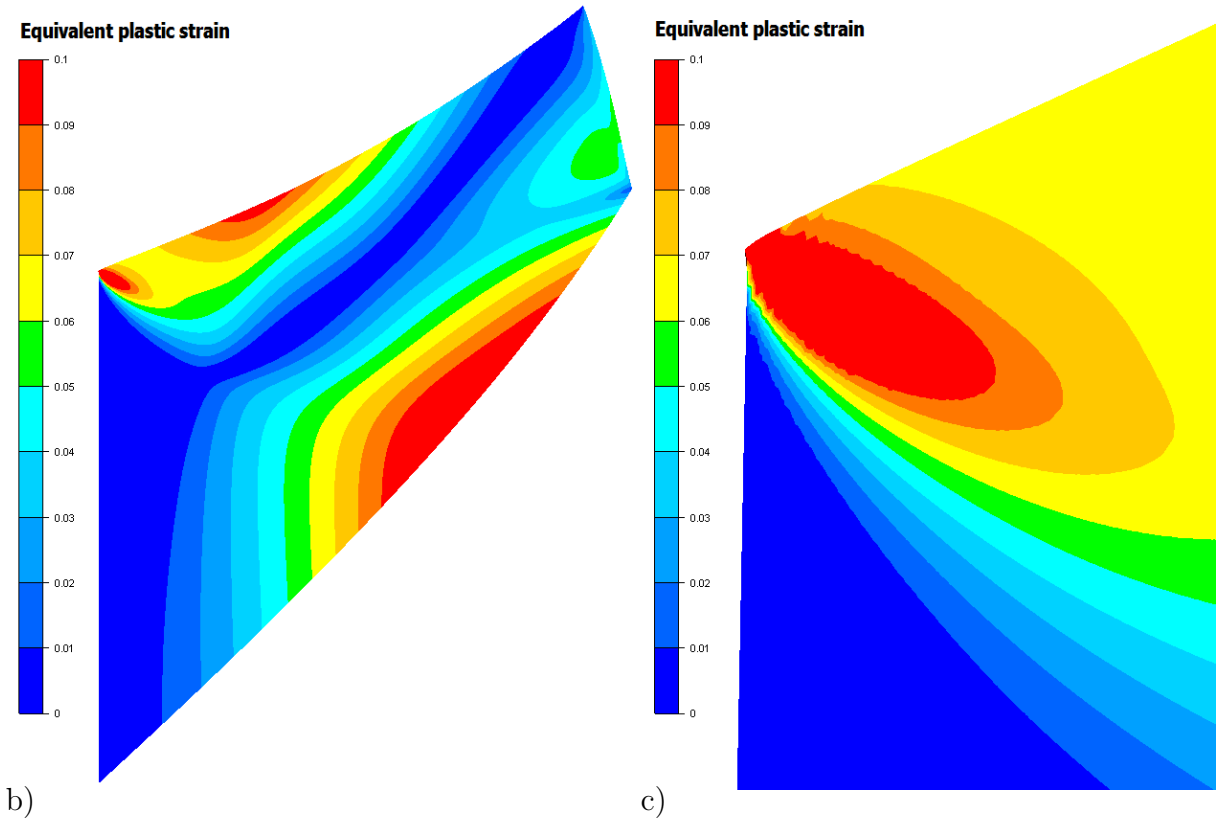

Figure 4. Cook's membrane problem – finite deformation plasticity: a) Energy norm errors. b) Equivalent plastic strain for the on the deformed configuration for the finest mesh with quartic Q_p/P_{p-1} NURBS at the final configuration. c) Close-up view of the equivalent plastic strain distribution around point A.

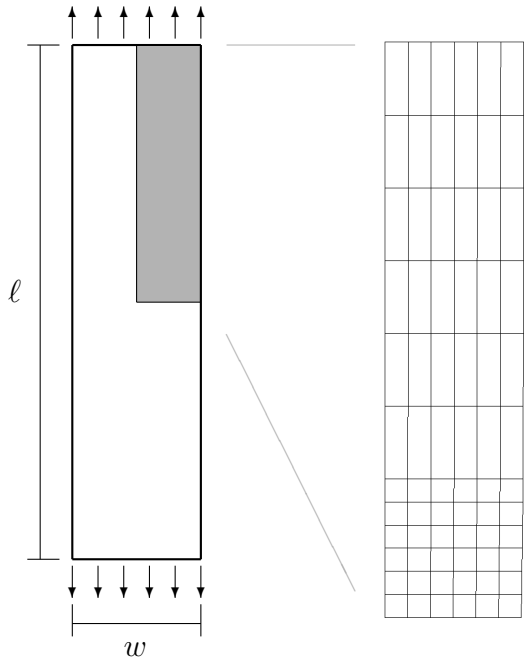

Length	:	ℓ	=	53.334
Width	:	w	=	12.826
Center width	:	w_c	=	$0.982w$
Bulk modulus	:	κ	=	164.206
Shear modulus	:	μ	=	80.1938
Initial yield stress	:	σ_0	=	0.45
Residual yield stress	:	σ_∞	=	0.715
Isotropic hardening	:	h	=	0.12924
Saturation exponent	:	β	=	16.93

Figure 5. Necking of an elastoplastic strip: Geometry, mesh and properties.

to the number of nodes, while for NURBS, the number of grid points corresponds to the number of control points in the width and length direction, respectively.

Figure 6a) shows the horizontal (necking) displacement of the bottom right corner of the discretized model (the shaded area in Figure 5) whereas Figure 6b) shows the reaction (necking) force versus prescribed (vertical) displacement of the top edge for the three different formulations for polynomial degree $p = 1, 2$ and 3 obtained with the 7×13 grid.

Except for the results obtained with the Q_p displacement formulation for the lowest polynomial degree ($p = 1$), which exhibit volumetric locking, the results for the three different formulations for $p = 2$ and 3 are nearly indistinguishable on the plots presented in Figure 6. In order to study the accuracy and convergence of the different formulations the coarsest 7×13 grid is successively refined into 13×25, 25×49 and 49×97 grid points, respectively.

As in the previous example, the analytical solution is not available, we therefore consider as reference solution the values obtained with a cubic Q_p/P_{p-1} mixed formulation with a very fine mesh with 5.9×10^5 dofs. The results in terms of the error in the necking force versus number of dofs are presented in Figure 7a). From Figure 7a) we observe that the NURBS Q_p solution is better than the corresponding Lagrange solution with the same polynomial order, and that the difference do not decrease notably as the polynomial order p of the basis functions is increased. We also notice that for all formulations the solution is improved as p increases. Also note that the accuracy and convergence of the NURBS Q_p solution coincide with the discontinuous Q_p/P_{p-1} mixed formulation when the polynomial order $p \geq 3$. Figure 7a) also documents that the discontinuous Q_p/P_{p-1} solution (as well as the NURBS Q_p solution for $p \geq 3$) is more accurate than the corresponding continuous Q_p/Q_{p-1} solution for all values of p.

Figure 7b) shows the von Mises stress distribution obtained with the finest 49×97 grid with NURBS $Q3/P2$ approximation at the final configuration.

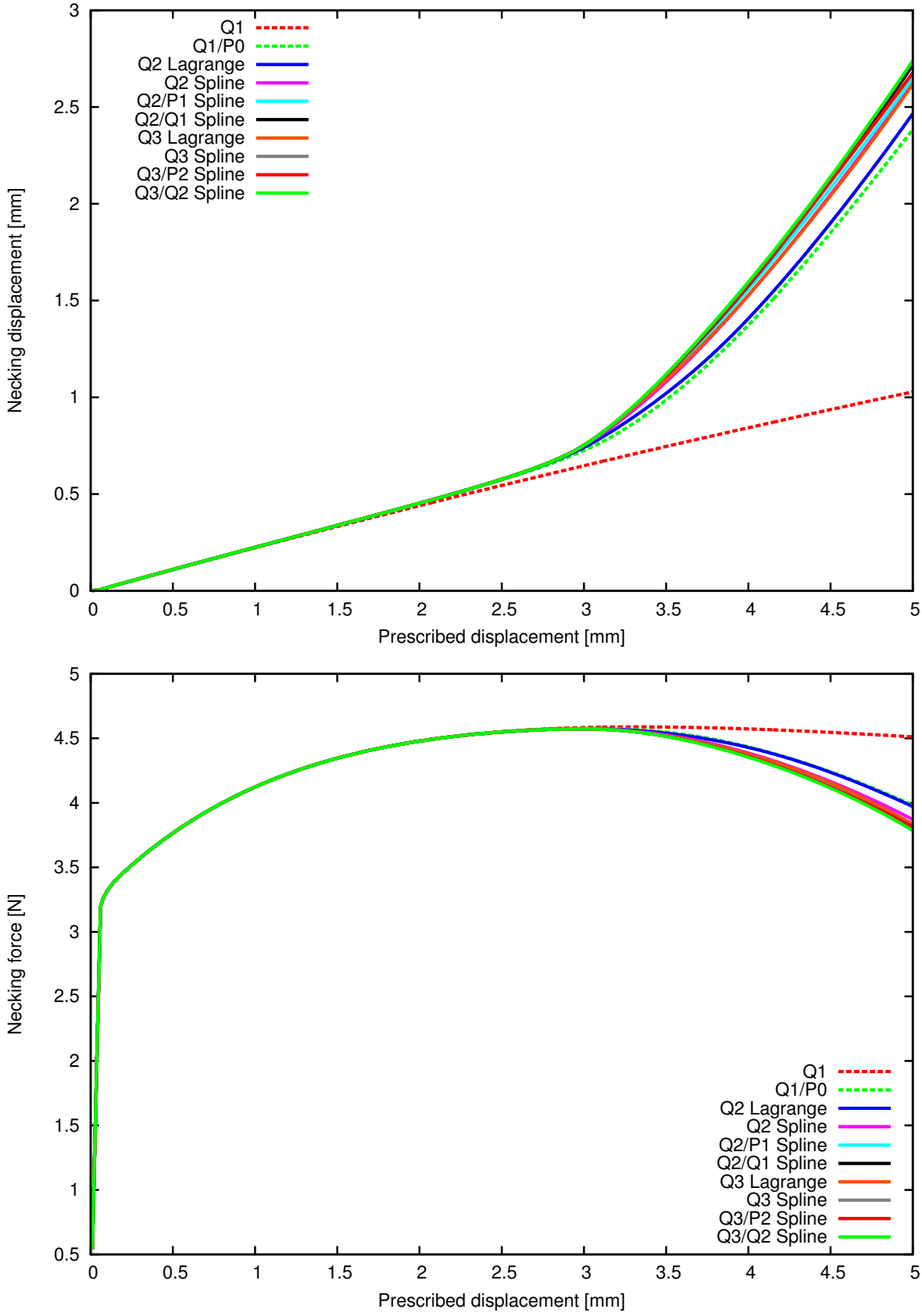

Figure 6. Necking of an elastoplastic strip with the 7×13 grid: a) Necking displacement. b) Necking force.

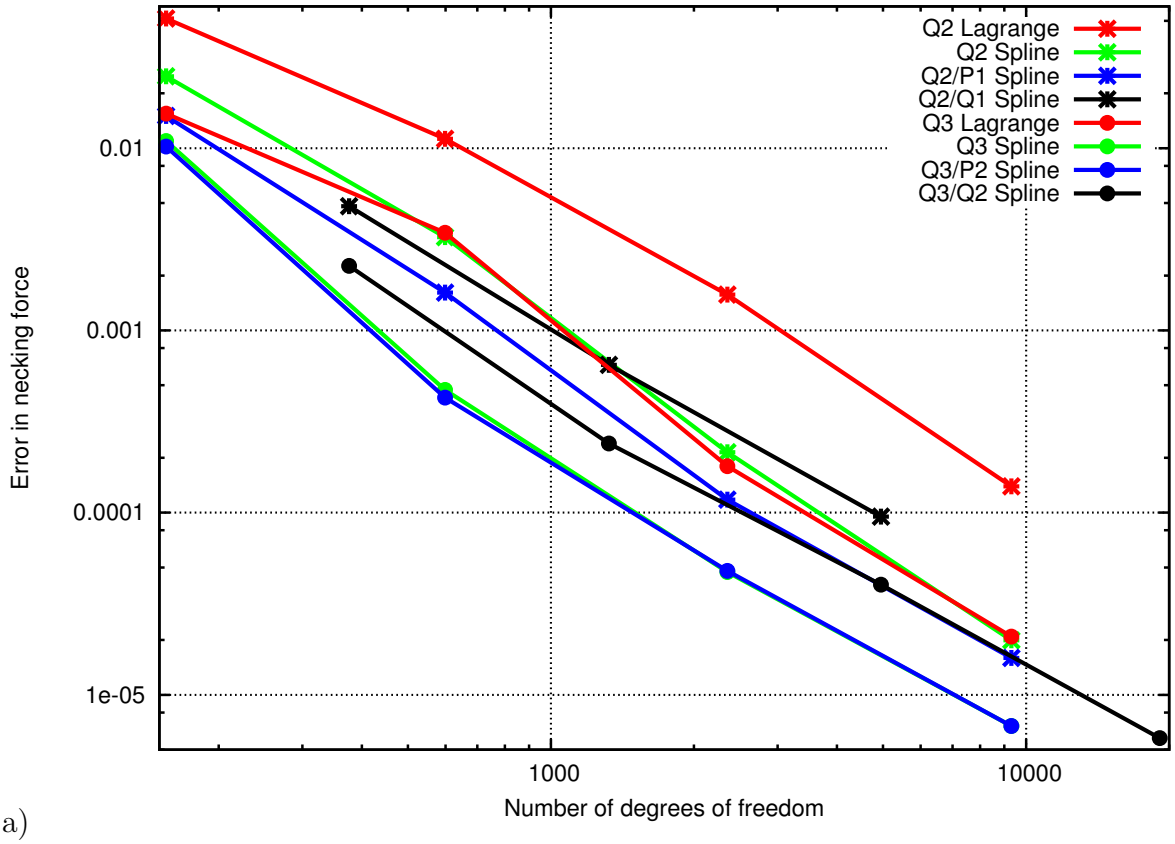

a)

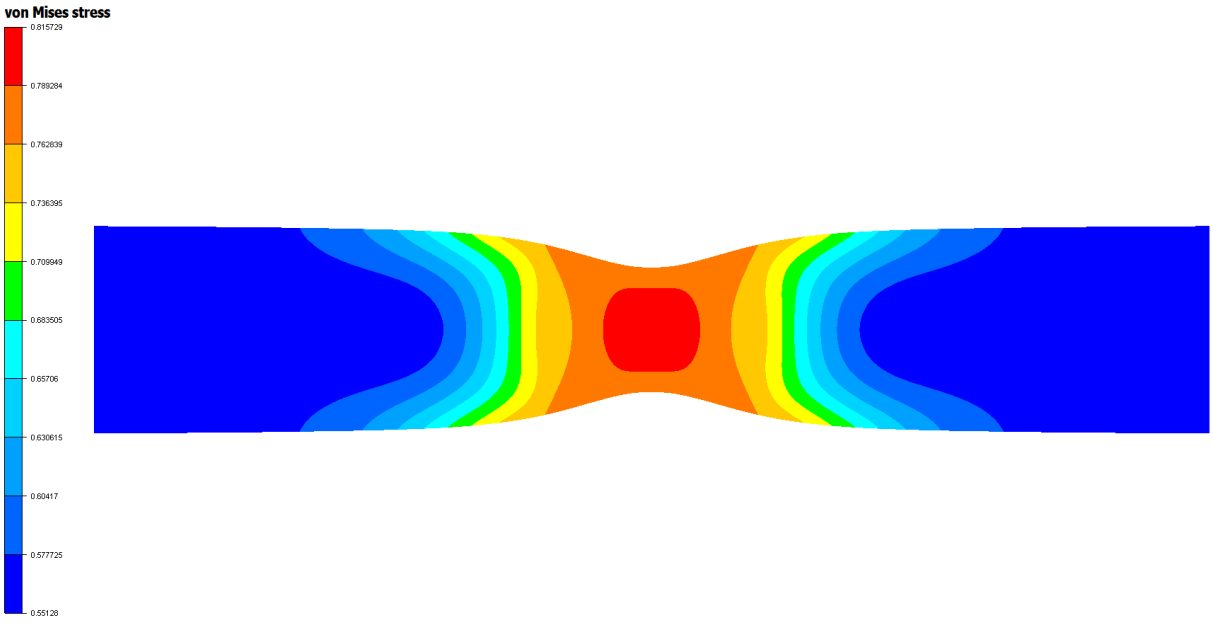

b)

Figure 7. Necking of an elastoplastic strip: a) Error in reaction force. b) von Mises stress distribution obtained with the finest 49×97 grid with NURBS $Q3/P2$ approximation at the final configuration.

Concluding Remarks

This paper has addressed the use of isogeometric analysis for finite deformation solid mechanics problems involving nearly incompressible hyperelastic and elastoplastic materials. Two different mixed formulations, based on a three-field Hu-Washizu variational principle, has been compared with a standard displacement formulation using NURBS as basis functions in the spatial discretization. The numerical results show that using NURBS is favorable compared with classical finite elements with Lagrange polynomials as basis functions. It also shows that the two mixed formulations are more accurate than the standard displacement formulation also for NURBS.

Acknowledgement

The authors acknowledge the financial support from the Norwegian Research Council and the industrial partners of the *ICADA*-project; Statoil, Det Norske Veritas and Ceetron, for this work. They also acknowledge the support from the other co-workers in the *ICADA*-project. They also would like to thank Professors T. J. R. Hughes (UT Austin) and R. L. Taylor (UC Berkeley) for fruitful discussions on the topic of the paper.

References

[1] J. A. Cottrell, T. J. R. Hughes, and Y. Bazilevs. *Isogeometric Analysis: Toward Integration of CAD and FEA*. John Wiley & Sons, Chichester, England, 2009.

[2] T. J. R. Hughes, J. A. Cottrell, and Y. Bazilevs. Isogeometric Analysis: CAD, Finite Elements, NURBS, Exact Geometry and Mesh Refinement. *Computer Methods in Applied Mechanics and Engineering*, 194:4135–4195, 2005.

[3] B. Szabó and I. Babuška. *Finite Element Analysis*. John Wiley and Sons, New York, NY, USA, 1991.

[4] B. Szabó, A. Düster, and E. Rank. The $p-$version of the Finite Element Method. In E. Stein, R. de Borst, and T. J. R. Hughes, editors, *Encyclopedia of Computational Mechanics, Volume 1: Fundamentals*. John Wiley & Sons, New York, 2004.

[5] T. Elguedj, Y. Bazilevs, V. M. Calo, and T. J. R. Hughes. $\overline{\mathrm{B}}$ and $\overline{\mathrm{F}}$ Projection Methods for Nearly Incompressible Linear and Non-linear Elasticity and Plasticity using Higher-order NURBS Elements. *Computer Methods in Applied Mechanics and Engineering*, 197:2732–2762, 2008.

[6] R. Echter and M. Bischoff. Numerical Efficiency, Locking and Unlocking of NURBS Finite Elements. *Computer Methods in Applied Mechanics and Engineering*, 199:374–382, 2010.

[7] J. C. Simo, R. L. Taylor, and K. S. Pister. Variational and Projection Methods for the Volume Constraint in Finite Deformation Elasto-plasticity. *Computer Methods in Applied Mechanics and Engineering*, 51:177–208, 1985.

[8] R. L. Taylor. Isogeometric Analysis of Nearly Incompressible Solids. *International Journal for Numerical Methods in Engineering*, 87:273–288, 2011.

[9] J. C. Simo and R. L. Taylor. Quasi-incompressible Finite Elasticity Stretches: Continuum Basis and Numerical Algorithms. *Computer Methods in Applied Mechanics and Engineering*, 85:273–310, 1991.

[10] O. C. Zienkiewicz and R. L. Taylor. *The Finite Element Method for Solid and Structural Mechanics*. Elsevier Butterworth and Heinemann, Oxford, England, 6th edition, 2005.

[11] F. Auricchio and R. L. Taylor. A Return-map Algorithm for General Associative Isotropic Elasto-plastic Materials in Large Deformation Regimes. *International Journal of Plasticity*, 15:1359–1378, 1999.

[12] J. C. Simo and T. J. R. Hughes. *Computational Inelasticity*. Interdisciplinary Applied Mathematics, volume 7. Springer, Berlin, Germany, 1998.

[13] I. Babuška. The Finite Element Method with Lagrangian Multipliers. *Numerische Matematik*, 20:179–192, 1973.

[14] F. Brezzi. On the Existence, Uniqueness and Approximation of Saddle-point Problems Arising from Lagrange Multipliers. *Revue Française d'Automatique Informatique Recherche Opérationelle*, 8(R-2):129–151, 1974.

[15] T. J. R. Hughes. *The Finite Element Method*. Prentice–Hall, Englewood Cliffs, NJ, USA, 1987.

[16] F. Auricchio, L. Beirão da Veiga, C. Lovadina, and A. Reali. An Analysis of some Mixed-Enhanced Finite Element for Plane Linear Elasticity. *Computer Methods in Applied Mechanics and Engineering*, 194:2947–2968, 2005.

[17] F. Auricchio, L. Beirão da Veiga, C. Lovadina, and A. Reali. The Importance of the Exact Satisfaction of the Incompressibility Constraint in Nonlinear Elasticity: Mixed FEMs versus NURBS-based Approximations. *Computer Methods in Applied Mechanics and Engineering*, 199:314–323, 2010.

[18] U. Brink and E. Stein. On some Mixed Finite Element Methods for Incompressible and Nearly Incompressible Finite Elasticity. *Computational Mechanics*, 19:105–119, 1996.

[19] J. M. A. César de Sá and R. M. Natal Jorge. New Enhanced Strain Elements for Incompressible Problems. *International Journal for Numerical Methods in Engineering*, 44:229–248, 1999.

[20] K. S. Chavan, B. P. Lamichhane, and B. I. Wohlmuth. Locking-free Finite Element methods for Linear and Nonlinear Elasticity in 2D and 3D. *Computer Methods in Applied Mechanics and Engineering*, 196:4075–4086, 2007.

[21] E. P. Kasper and R. L. Taylor. A Mixed Enhanced Strain Method. Part II: Geometrically Nonlinear Problems. *Computers and Structures*, 75:251–260, 2000.

[22] O. Klass, A. Maniatty, and M. S. Shephard. A Stabilized Mixed Finite Element Method for Finite Elasticity. Formulation for Linear Displacement and Pressure Interpolation. *Computer Methods in Applied Mechanics and Engineering*, 180:65–78, 1999.

[23] K. B. Nakshatrala, A. Masud, and K. D. Hjelmstad. On Finite Element Formulations for Nearly Incompressible Linear Elasticity. *Computational Mechanics*, 41:547–561, 2008.

[24] S. Reese, P. Wriggers, and B. D. Reddy. A New Locking-free Brick Element Technique for Large Deformation Problems in Elasticity. *Computers and Structures*, 75:291–304, 2000.

[25] E. A. de Souza Neto, D. Peric, M. Dutko, and D. R. J. Owen. Design of Simple Low Order Finite Elements for Large Strain Analysis of Nearly Incompressible Solids. *International Journal of Solids and Structures*, 33:3277–3296, 1996.

[26] E. A. de Souza Neto, F. M. Andrade Pires, and D. R. J. Owen. F-bar-based Linear Triangles and Tetrahedra for Finite Strain Analysis of Nearly Incompressible Solids. Part I: Formulation and Benchmarking. *International Journal for Numerical Methods in Engineering*, 62:353–383, 2005.

[27] J. C. Simo and F. Armero. Geometrically Non-linear Enhanced Strain Mixed Methods and the Method of Incompatible Modes. *International Journal for Numerical Methods in Engineering*, 33:1413–1449, 1992.

[28] S. Glaser and F. Armero. On the Formulation of Enhanced Strain Finite Elements in Finite Deformation. *Engineering with Computers*, 14:759–791, 1997.

[29] B. Ramesh and A. Maniatty. Stabilized Finite Element Formulation for Elastic-plastic Finite Deformations. *Computer Methods in Applied Mechanics and Engineering*, 194:775–800, 2005.

[30] J. C. Simo. A Framework for Finite Strain Elastoplasticity based on Maximum Plastic Dissipation and the Multiplicative Decomposition: Part I. Continuum Formulation. *Computer Methods in Applied Mechanics and Engineering*, 66:199–219, 1988.

[31] J. C. Simo. A Framework for Finite Strain Elastoplasticity based on Maximum Plastic Dissipation and the Multiplicative Decomposition: Part II. Computational Aspects. *Computer Methods in Applied Mechanics and Engineering*, 68:1–31, 1988.

[32] E. N. Dvorkin and A. P. Assanelli. Implementation and Stability Analysis of the QMITC-TLH Elasto-plastic Finite Strain (2D) Element Formulation. *Computers and Structures*, 75:305–312, 2000.

[33] C. Agelet de Saracibar, M. Chiumenti, Q. Valverde, and M. Cervera. On the Orthogonal Subgrid Scale Pressure Stabilization of Finite Deformation J2 Plasticity. *Computer Methods in Applied Mechanics and Engineering*, 195:1224–1251, 2006.

Kjell Magne Mathisen, Siv Bente Raknes
Department of Structural Engineering
Norwegian University of Science and Technology, NO-7491 Trondheim, Norway
`kjell.mathisen@ntnu.no, siv.bente.raknes@ntnu.no`

Knut Morten Okstad, Trond Kvamsdal
Department of Applied Mathematics
SINTEF ICT, NO-7465 Trondheim, Norway
`knut.morten.okstad@sintef.no, trond.kvamsdal@sintef.no`